Superconductor Science and Technology

PAPER

In-field critical current and pinning mechanisms at 4.2 K of Zr-added REBCO coated conductors

To cite this article: Eduard Galstyan *et al* 2020 *Supercond. Sci. Technol.* **33** 074007

IOP Publishing Superconductor Science and Technology
Supercond. Sci. Technol. **33** (2020) 074007 (12pp) https://doi.org/10.1088/1361-6668/ab90c6

In-field critical current and pinning mechanisms at 4.2 K of Zr-added REBCO coated conductors

Eduard Galstyan[1], Rudra Pratap[1], Goran Majkic[1], Mehdi Kochat[1], Dmytro Abraimov[2], Jan Jaroszynski[2] and Venkat Selvamanickam[1]

[1] Department of Mechanical Engineering, Advanced Manufacturing Institute and Texas Center for Superconductivity, University of Houston, Houston, TX 77204, United States of America
[2] Applied Superconductivity Center, National High Magnetic Field Laboratory, Florida State University, Tallahassee, Florida 32310, United States of America

E-mail: selva@uh.edu

Received 14 February 2020, revised 8 April 2020
Accepted for publication 6 May 2020
Published 3 June 2020

Abstract

The critical current and pinning mechanisms at 4.2 K have been studied over a magnetic field range of 0–14 T for Zr-added (0, 5 and 15 mol.%) $REBa_2Cu_3O_{7-x}$ (REBCO and RE = rare earth) coated conductors fabricated by advanced metal organic chemical vapor deposition (A-MOCVD). It is found that the (Ba + Zr)/Cu content in Zr-added (5 and 15 mol.%) REBCO affects the critical current at 77 K, 0 T as well as density, continuity and shape of $BaZrO_3$ (BZO) self-assembled nanocolumns and RE_2O_3 in-plane precipitates that significantly enhance the pinning force density $Fp(H)$ as well as isotropic pinning landscape at 4.2 K. In addition to bell-shape dependence of critical current density, J_c, at 4.2 K with (Ba + Zr)/Cu content we observed an unusual $Fp(H)$ behavior correlated to particular type of pinning centers, morphology and distribution that have been revealed by TEM microstructure analysis. By fitting the Dew–Hughes equation of the pinning force density $Fp(H)$ at 4.2 K we extract the scaling behaviors of the $Fp(H)$ associated with the competition of pinning mechanisms driven by vertically-aligned BZO nanorods and in-plane RE_2O_3 pinning defects. This result sheds light on approaches towards interactive control of strong and isotropic pinning centers in Zr-added $REBa_2Cu_3O_{7-x}$ (REBCO and RE = rare earth) coated conductors, and especially understanding the correlation between microstructural characteristics and vortex pinning mechanisms at 4.2 K in high magnetic fields.

Keywords: REBCO, coated conductor, metal organic chemical vapor deposition (MOCVD), critical current density, pinning, microstructure, transmission electron microscopy (TEM)

(Some figures may appear in colour only in the online journal)

1. Introduction

In recent years, there has been a strong interest in using $REBa_2Cu_3O_{7-x}$ (REBCO, RE-rare earth element) coated conductors at low temperatures of 4.2–20 K and high magnetic fields for applications such as accelerator magnets for high-energy physics, fusion magnets, and superconducting magnetic energy storage systems (SMES) [1–9]. REBCO coated conductors made by metal organic chemical vapor deposition (MOCVD) and pulsed laser deposition (PLD) with incorporated artificial pinning centers (APCs) exhibit the critical current density (J_c) over 8 MA cm^{-2} and pinning force density (Fp) over 1.4 TN m^{-3} at 4.2 K and 20 T [10–12]. Among the various methods to enhance the pinning characteristics in REBCO, $BaMO_3$ (M = Zr, Hf) self-assembled nanorods, primarily oriented along the c-axis of REBCO, are one of the most effective APCs [13–19].These nanocolumns can be grown along entire thickness of film and are about 3–8 nm in diameter, comparable to coherence length on the a-b plane. Record high J_c over 12 MA cm^{-2} and pinning force

of 1.7 TN m^{-3} at 4.2 K in a magnetic field of 14 T have been reported by our group for 15 mol.% Zr -added REBCO 4+ μm thick film made by Advanced MOCVD technique, which is based on direct ohmic heating of a suspended substrate tape and laminar precursor cross flow [20–22]. It has been possible to grow even 5 μm thick films with a homogeneous microstructure free of a-axis grains film in a single pass by A-MOCVD because of excellent temperature control and uniform precursor flow. It has been reported that $BaZrO_3$ (BZO) nanocolumns provide strong correlated pinning along the *c*-axis and introduce the weak point defects such as oxygen vacancies, dislocations and those due to the strain induced by lattice mismatch between BZO nanorods and REBCO matrix that enhance the J_c over a wide range of magnetic field directions [23]. Depending on pinning strength, vortex spacing, and pin density at low temperature, several mechanisms such as strong and weak pinning have been discussed; however varied reports leave several unresolved questions. One question is about the transition mechanism between the strong correlated and weak uncorrelated pinning with field at temperatures below 20 K and its dependence on the dimensionality of pinning defects such as nanorods and nanoparticles. Another unclear characteristic is α value, a parameter that is related to the strength of flux pinning in power-law dependence, $I_c \sim H^{-\alpha}$. A wide range of $\alpha = 0.69$–0.89 has been observed for Zr-added REBCO films [19]. Recently, it has been reported that α value for REBCO containing RE_2O_3 precipitates decreases with temperature and approaches to 0.5 at 5 K [24]. The common conclusion is that there is no universal value for α and power-law fit for $J_c(H)$ is not always valid. In addition to these unresolved questions, there is generally a dearth of reports on the in-field critical current of REBCO coated conductors at low temperatures.

In this work we studied the magnetic critical current density (J_c) at 4.2 K and wide magnetic field range 0–14 T applied perpendicular to plane of Zr-added (Gd,Y)BCO tape. All studies focused only on thick (4 + μm) films that we have demonstrated in our A-MOCVD tool. This tool enables growth of thick REBCO films without degradation in J_c, resulting in values between 2.5 and 3.8 MA cm^{-2} at 77 K, 0 T, over 15 MA cm^{-2} at 30 K, 3 T and 0.5 MA cm^{-2} at 4.2 K, 14 T [17, 20]. The main parameters explored in this study are Zr content (0, 5 and 15% Zr addition) and Ba/Cu stoichiometry.

2. Experimental details

The Advanced MOCVD method was used to fabricate (Gd,Y)BCO thick (4+ μm) films with 0, 5 and 15 mol.% Zr addition and different Ba content [21, 22]. The film growth temperature range and reactor pressure were 800 °C–820 °C, 10^{14} ppm and 1.9 Torr, respectively. The direct ohmic heating and laminar precursor flow in Advanced MOCVD enable excellent temperature control, rapid thermal response and direct monitoring of tape temperature. All (Gd,Y)BCO films were grown using a constant Gd:Y ratio (0.6:0.6) while the Ba molar ratio in (Gd,Y)BCO superconducting tapes was varied over a range of 1.8−2.35. The (Ba + Zr)/Cu content in 0, 5 and 15% mol.% Zr-added (Gd,Y)BCO films was determined from the composition analysis by inductively coupled plasma mass spectroscopy (ICP-MS). (Ba + Zr)/Cu ratio has been previously shown to be strongly correlated with in-field critical current [16, 25].

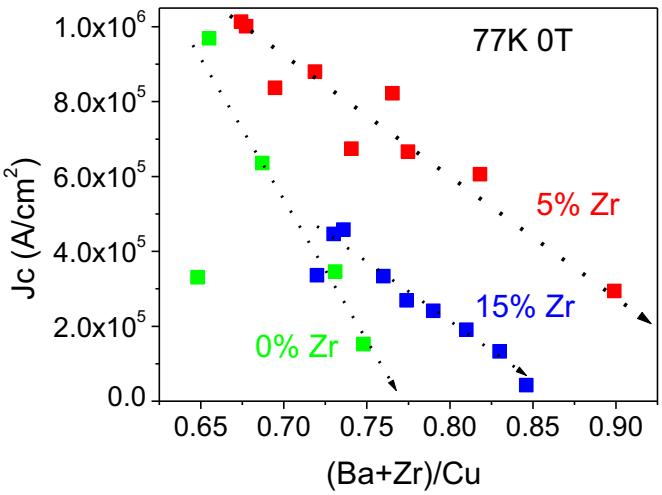

Figure 1. Magnetization J_c at 77 K and 0 T as a function of (Ba + Zr)/Cu for 0, 5 and 15% Zr-added (Gd,Y)$Ba_2Cu_3O_{7-x}$ tapes as function of (Ba + Zr)/Cu content.

Contact-free magnetic measurements were conducted by a vibrating sample magnetometer (VSM), Quantum Design DynaCool PPMS with a 14 T maximum field. All samples, with dimensions 3.2 × 3.2 mm^2 cut from the 12 mm tapes, were measured with the magnetic field applied perpendicular to Zr/(Gd,Y)BCO tapes. The critical current density J_c was obtained from measurements of hysteretic magnetization loops $M(H)$. These data were analyzed using the Bean critical model for a rectangular sample with sides, $b > a$, where the current density (in CGS units) is given by $J_c = 20\ \Delta M/a\ (1 - a/3b)$ [26, 27]. In the VSM, a magnetic field sweep rate of 200 Oe s^{-1} was used, which corresponds to an electric field E ≈ 10^{-7} V cm^{-1} defined by E = (a/4) (dB/dt) [24, 28]. Transport critical current measurement at 77 K, 0 T was conducted in liquid nitrogen using a 4-probe method. The in-field transport critical currents at 4.2 K in high magnetic fields up to 32 T were measured in a 31.2 T solenoid magnet at NHMFL. An electric field criterion of E ≈ 1 μV cm^{-1} was used to define transport critical current, I_c. Transmission electron microscopy (TEM) studies were performed on a JEOL 2000FX microscope.

3. Results and discussion

We first explored the effect of Zr content and Ba/Cu ratio on the resulting 77 K, self-field behavior. The magnetization critical current density (J_c) at 77 K, 0 T as a function of (Ba + Zr)/Cu content for (Zr = 0, 5 and 15 mol.%) REBCO tapes is shown in figure 1. The J_c (77 K, 0 T) reduces almost linearly from 0.95 to 0.2 MA cm^{-2} for the reference undoped (Zr = 0) samples, while REBCO tapes with 5 and 15 mol.

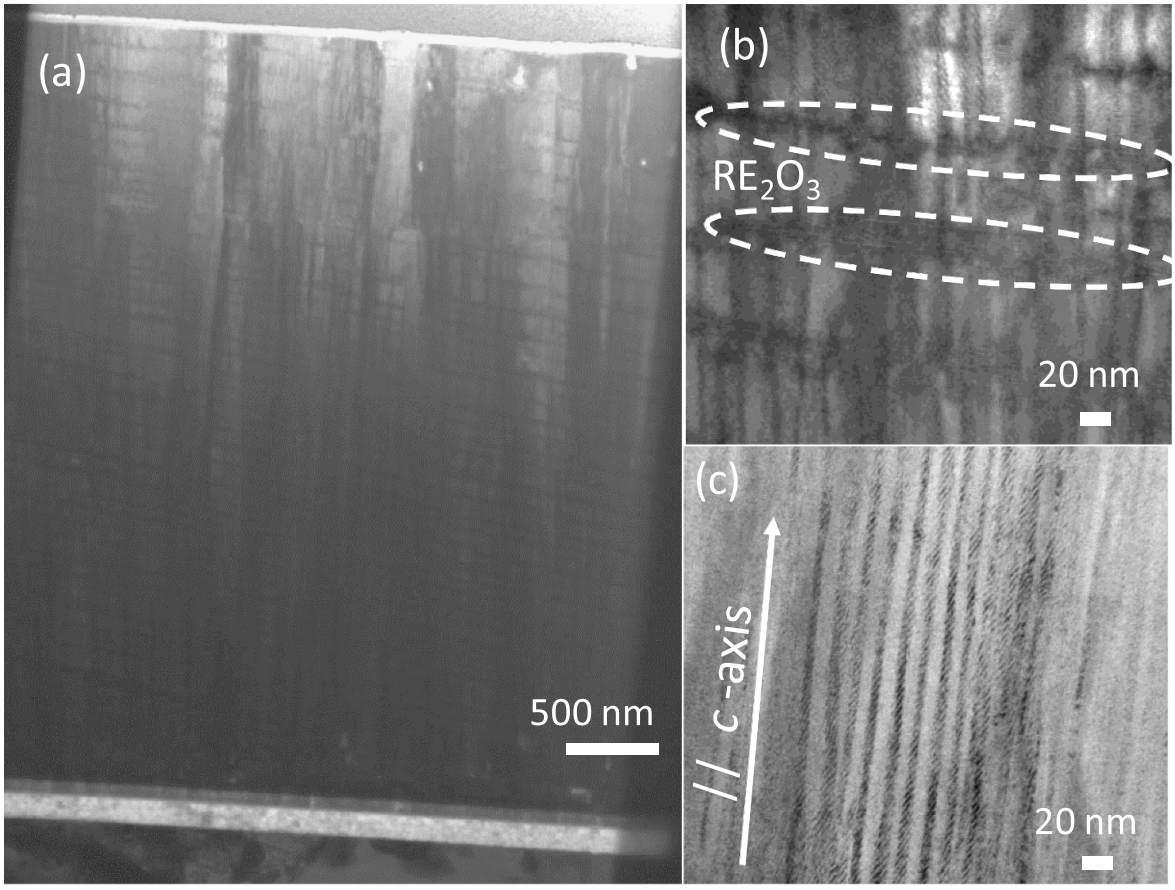

Figure 2. A typical cross section microstructure of Zr-added (Gd,Y)BCO sample at low magnification (a). Cross section microstructure of 15 mol. % Zr-added (Gd,Y)BCO with low (Ba + Zr)/Cu = 0.72 content (b) and high (Ba + Zr)/Cu = 0.846 content (c). In figure 2 (b) the in-plane RE_2O_3 precipitates are indicated by dashed lines.

% Zr addition show J_c (77 K, 0 T) decreasing from 1 to 0.3 MA cm^{-2} and from 0.4 to 0.04 MA cm^{-2} respectively.

Transport J_c measured on the same samples show higher values by factor of ∼2 than magnetization J_c due to the difference in voltage criteria used to define J_c. This difference also depends on uniformity of samples and index n value of the power law characteristic of each sample [22, 28, 29].

Figure 1 shows that the achievable J_c in 0 and 5% Zr films is the highest in Cu-excess samples with (Ba + Zr)/Cu ∼ 0.66. However, it is seen that J_c degrades at much lower rate in 5% Zr samples as (Ba + Zr)/Cu content is increased. The slope of J_c vs. (Ba + Zr)/Cu behavior is practically the same in 5 and 15% Zr samples, while the J_c of samples with no Zr addition deteriorates at a higher rate. In addition, the 15% Zr samples have a lower J_c than the 5% Zr samples. This observation is consistent with reports on Zr/(Gd,Y)BCO films with variable Ba and Zr content [16, 30–32]. It has been found that (Gd,Y)BCO *c*-axis lattice parameter strongly depends upon the Zr and Ba/Cu concentration in REBCO superconductor tapes. The reduction of J_c at 77 K, 0 T with a high level of Zr addition is attributed to in-plane texture degradation and increasing of *c*-axis lattice parameter. In Ba-rich REBCO superconductor tapes, there are suggestions that the excess Ba content occupies the yttrium (Y) sites which due to the larger ionic radius of Ba in comparison with Y, results in an expansion of the REBCO *c*-axis lattice parameter [33]. On the other hand, deficiency of Ba in the film can cause a sharp drop of critical current as shown in figure 1 for 0% Zr with Ba/Cu = 0.65, due to formation of *a*-axis-oriented grains and secondary phases, such as CuO. Another factor known to affect the self-field J_c and in-field performance at B||*ab* plane is the concentration of rare-earth elements (Y, Gd) formed in superconducting film as RE_2O_3 (REO) nanoprecipitates [34]. In the samples studied in the current work, the RE concentration is fixed at 1.3, resulting in nominal 0.3 RE excess relative to REBCO unit cell available for formation of REO precipitates. However, the density of REO nanoparticles, as will be shown in microstructural analysis, reduces with increasing the (Ba + Zr)/Cu content in the films, which is one of the possible causes for the reduction of J_c at 77 K, 0 T.

A low magnification view of a typical cross-section microstructure of Zr-added REBCO films made by A-MOCVD is shown in figure 2. Homogeneous 4+ μm thick films free of a-axis grains can be grown in a single pass by A-MOCVD. We observe uniform distribution of BZO nanorods along *c*-axis. The BZO nanorod areal density determines the matching field for flux pinning and is desired to be as high as achievable without deterioration of the underlying REBCO structure. Among over 10 samples studied by TEM, a remarkable observation for 5 and 15 mol.% Zr-added samples is

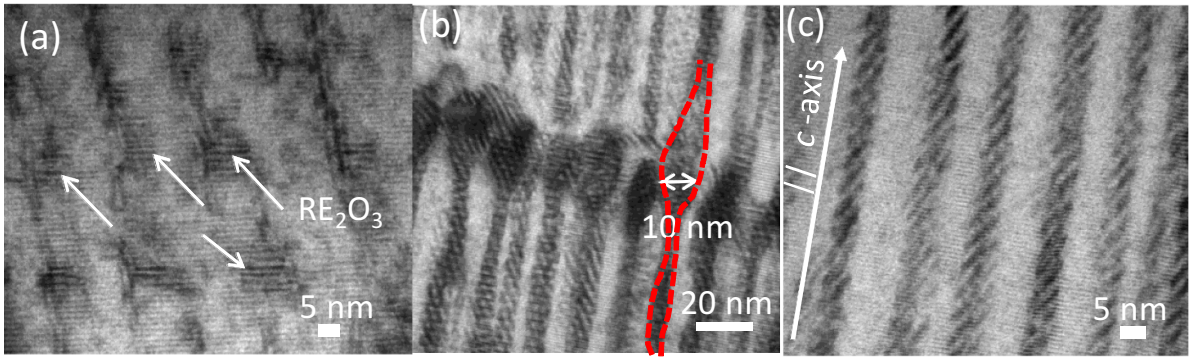

Figure 3. Cross section microstructures of 15% Zr-added (Gd,Y)BCO samples with different compositional ratio (Ba + Zr)/Cu: low-0.72 (a), moderate-0.76 (b) and high-0.85 (c). The bottle-shaped BZO nanorods with alternating narrow and wide sections are marked by dashed lines.

the high density of REO precipitates homogeneously dispersed along the *ab* plane for samples with low Ba content [(Ba + Zr)/Cu = 0.72] (figure 2(b)), while the films with high Ba level [(Ba + Zr)/Cu = 0.846] do not reveal any appreciable density of REO (figure 2(c)).

TEM cross section microstructure analysis of 15 mol.% Zr-added films shows an increasing spacing between in-plane REO precipitates from 56 to 950 nm with increasing of (Ba + Zr)/Cu content from 0.66 to 0.85. An increase of the Ba concentration in the precursor leads to increase of the Ba/Cu stoichiometry in the films. For Zr = 0, 5 and 15%, the nominal perfect Ba/Cu stoichiometry is 2/3, 2.05/3 and 2.15/3, respectively, and accounts for the amount of extra Ba content needed to form $BaZrO_3$. The corresponding (Ba + Zr)/Cu stoichiometric values are 0.667, 0.7 and 0.767, respectively. At (Ba + Zr)/Cu values lower than the listed values, the films are Ba-deficient, or correspondingly Cu-rich. This is a possible cause for formation of a-oriented REBCO grains, nucleating from Cu-oxide precipitates. Simultaneously with Ba deficiency, an excess RE content is available for the formation of REO precipitates. The size of RE_2O_3 particles might vary from 3 to 10 nm depending on the film growth temperature and time as well as the variation of Ba in the film composition. The REO particles as shown in figures 2(b) and 3(a) can disrupt BZO continuity along the *c*-axis of REBCO films, resulting in an array of shorter, segmented nanorods.

Figure 3 shows the cross-sectional morphology of 15 mol% Zr-added films made with low Ba = 2.0, moderate Ba = 2.15 and large Ba = 2.35 in the precursor that correspond to (Ba + Zr)/Cu compositional ratio in films of 0.72, 0.76 and 0.85 respectively. The films with 5% Zr addition have similar microstructures as those shown in figure 3, but with different nanorod density.

It can be seen that increasing the Ba content affects the continuity, morphology and density of BZO nanorods. The average diameter of BZO nanorods appears to slightly increase, from ∼4 to ∼6 nm between the two extremes. The near independence of BZO diameter size on doping concentration in REBCO film with sufficiently high BZO content has been proposed by Wu *et al* based on calculation of elastic energy of the strained lattice [35]. In the Ba-2.0 sample as shown in figure 3(a), the BZO nanocolumns appear partially interrupted by the REO precipitates present along the *ab* plane. In REBCO films where REO and BZO are incorporated, additional defects such as stacking faults are also present and might act as additional pinning centers [36, 37]. The $BaZrO_3$ nanocolumns in 15 mol.% Zr added film made with Ba = 2.15 precursor show a modulation of the nanorod diameter along the length. The nanorods feature bottle-shaped periodic modulations, which increase the nanorod diameter locally to 10–12 nm diameter, that appear along the whole thickness of the 4+ μm REBCO films. Such periodic instabilities in diameter are not currently predicted by any existing nanorod growth theory and the precise mechanism behind it is not clear at the moment. The microstructure of the film made with high Ba = 2.35 precursor content does not show any bottle-shaped features in BZO nanocolumns. In addition, there are no significant traces of any RE_2O_3 precipitates. The nanocolumns appear continuous and straight. Furthermore, the nanorod diameter appears larger than that of the low Ba sample. While the nanorod diameter is more difficult to evaluate accurately from the presented cross-section micrographs compared to the estimate of nanorod density from plan-view nanorod count, the nanorod diameter is estimated at 4–4.8 nm for Ba = 2, 5–7 nm for Ba = 2.15 in the narrow sections and ∼15 nm in the bottle-shape sections, and 8–9 nm for Ba = 2.35.

The spacing between BZO nanorods of 5 and 15 mol. % Zr−added REBCO tapes with different Ba content is shown in figure 4. The square symbols denote estimates of nanorod density from the peak in pinning force vs applied field as measured at 65 K by VSM magnetometry. The corresponding estimate of nanorod density from plan-view TEM micrographs is denoted with star and circular symbols. Up to the matching fields, every flux line can be pinned by an individual BZO nanocolumn. Our recent publication shows that matching fields of Zr-added REBCO films obtained from magnetization curves at 65 K agree well with those evaluated from the average spacing of BZO nanocolumns [38]. This correlation at 65 K was observed for over 20 Zr-added REBCO samples measured over a wide temperature range.

Figure 4 demonstrates that the spacing between BZO nanocolumns decreases with increasing Ba content, implying an

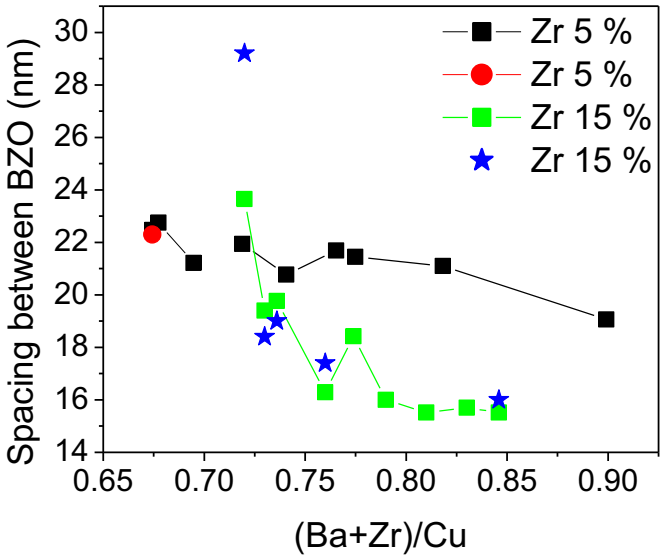

Figure 4. Spacing between BZO nanorods of 5 and 15 mol. % Zr-added $(Gd,Y)Ba_2Cu_3O_{7-x}$ films as a function of (Ba + Zr)/Cu content. The square symbols represent the data obtained from matching field characteristics measured over $J_c(H)$ at 65 K. The circular and star symbols correspond to TEM plan view microstructure analyses.

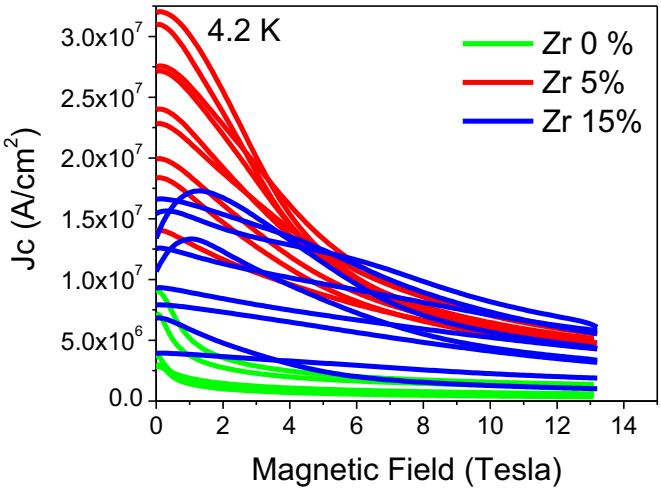

Figure 5. Field dependence of J_c at 4.2 K and B||c for 0, 5 and 15 mol.% Zr-added REBCO tapes with Ba molar ratio in the precursor varied over 1.8 − 2.35.

increase in nanorod content. It is more prominent for 15 mol.% added films, where the spacing reduces from 24 nm for Ba = 2.0, (Ba + Zr)/Cu = 0.72 down to 16 nm for Ba = 2.35, (Ba + Zr)/Cu = 0.85. On the other hand, films with 5 mol.% Zr addition show moderate changes in BZO spacing, decreasing from 23 nm for Ba = 2.0, (Ba + Zr)/Cu = 0.67 down to 19 nm for Ba = 2.3, (Ba + Zr)/Cu = 0.9. This observation is consistent with earlier published work where increase of (Ba + Zr)/Cu leads to reduction of BZO-to-REBCO *c*-lattice mismatch that promotes formation of BZO nanorods with higher density [16].

The pinning mechanism at temperatures below 30 K is expected to be significantly different from that at high temperatures due to changes in coherence length of vortices and effects associated with temperature fluctuation [23]. At lower temperatures and high magnetic fields, dense uncorrelated pinning centers are mostly caused by weak points through oxygen vacancies and those that arise from lattice mismatch strain fields between REBCO matrix and pinning centers such as BZO nanorods and REO nanoparticles [23, 39–42]. Hence, it is important to find out the mechanisms that can optimize the pinning landscape in order to achieve the high performances at lower temperatures in low to high magnetic field regimes.

Figure 5 shows the magnetic field dependence of J_c at 4.2 K in the field orientation $B\|c$, for the 0, 5 and 15 mol.% Zr-added REBCO films with Ba molar ratio in the precursor varied over 1.8–2.35. The J_c of the reference undoped samples over the field range of 0–4 T is around 4 MA cm^{-2} which is lower by a factor of 5 and 3 compared to 5 and 15 mol.% Zr-added samples respectively. At higher magnetic fields, the factor is around 8. Another remarkable observation is that at lower fields of 0–5 T, REBCO tapes with 5 mol.% Zr addition show higher J_c than 15 mol. % Zr samples by an average factor of 2.5, while at fields above 5 T, the best 15% Zr-added samples outperform 5% Zr added samples.

The tapes with higher Zr levels are likely more degraded due to increased *c*-axis lattice parameter and therefore show lower critical current at low field where the effect of weak pinning center is not dominating. At 4.2 K and magnetic fields above 8 T, the difference in J_c of 5 and 15% Zr-added samples continuously reduces suggesting that isotropic point defects are dominating the pinning mechanism rather than BZO nanorods, which is in a good agreement with earlier published work [39]. Data in figure 5 also reveals that over the magnetic field range 0–4 T, the rate of decrease in critical current with increasing magnetic field is stronger for 5 mol. % Zr added tapes while at high magnetic fields, the rate for both Zr-added tapes is almost identical. It is worth to note that the mean value of the lift factor, defined as the ratio of J_c at a given temperature and field to J_c at 77 K, 0 T, of undoped samples is around 8 in low magnetic fields, and is around 33 and 50 respectively for 5 and 15 mol.% Zr added tapes. At high magnetic fields, the mean lift factor is 1.5, 6, and 13 for 0, 5 and 15 mol.% Zr added REBCO tapes respectively. The high lift factor value without severe degradation of self-field J_c at 77 K is an indication of strongly active flux pinning mechanism. It is also evident from figure 5 that the (Ba + Zr)/Cu content variation in 5 and 15 mol.% Zr-added REBCO tapes strongly affects the $J_c(H)$ distribution. At low fields, for example at 2 T, the samples with 5 and 15 mol.% Zr addition show a range of J_c from 12 to 27 MA cm^{-2} and 4–16 MA cm^{-2} respectively, while for undoped samples the range is smaller, from 1.4 to 3.6 MA cm^{-2}.

Among the 23 samples presented in the figure 5, two samples with 15 mol.% addition show anomaly of a peak in J_c at a low magnetic field, around 1.2 T. All samples were measured by using the same magnetization sequence, so additional study of these two samples is needed to understand the nature of the observed J_c peak. It is worth noting that a similar behavior in $J_c(H)$ i.e. an increase in J_c with increasing

magnetic field known as fishtail (or second peak) effect has been reported previously, but the interpretation of this phenomenon is still rather controversial [43, 44].

The correlation between the $J_c(H)$ at 4.2 K and (Ba + Zr)/Cu content of 0, 5 and 15 mol.% Zr-added REBCO tapes is shown in figure 6. It can be seen that the J_c for reference and Zr-added samples at a high magnetic field of 13 T follows a bell-shaped behavior as a function of (Ba + Zr)/Cu content. A pronounced peak is observed for tapes with 15% Zr addition (figure 6(a)). Increasing of (Ba + Zr)/Cu content from 0.72 to 0.774 leads to an improvement of J_c by factor of 6 which approaches 6.3 MA cm^{-2}, while the further increase of (Ba + Zr)/Cu from 0.774 to 0.85 drops the J_c to 0.9 MA cm^{-2}. At 13 T, the peak J_c, is observed for the 15% Zr tape with Ba = 2.15 nominal level in precursor, (Ba + Zr)/Cu = 0.774. For this tape, the spacing between $BaZrO_3$ nanorods is 18 nm. Among films with 5% Zr, the peak J_c at 13 T has been observed for Ba = 2, (Ba + Zr)/Cu = 0.74 where the spacing between $BaZrO_3$ nanorods is 21 nm.

In figure 6(a) is shown that the highest J_c in the field range of 7–13 T occurs for the same 15% Zr tape with (Ba + Zr)/Cu content of 0.774, while J_c max at fields below 7 T happens in films with a lower (Ba + Zr)/Cu content, less than or equal to 0.76. Similarly, the optimum (Ba + Zr)/Cu content in 5 mol.% Zr added tapes for the maximum critical current decreases with decreasing magnetic field. So, by tailoring the composition, the performance of REBCO tapes can be customized to the magnetic field relevant to the application. In figure 6(c) the dependence of J_c at 9 T and 13 T of undoped, 5 and 15 mol. % Zr-added REBCO tapes on (Ba + Zr)/Cu content is compared. At 13 T, REBCO tapes with Zr = 0, 5, and 15 addition show $J_{c\,max}$ = 1.4, 5.7 and 6.3 MA cm^{-2} respectively, and at 9 T, they exhibit $J_{c\,max}$ = 1.6, 7.8 and 8.9 MA cm^{-2}. While the 15% Zr-added tapes show the highest J_c, the 5% Zr-added tapes exhibit a high J_c over a wide range of (Ba + Zr)/Cu content. Such a broad window will be valuable for consistency and uniformity in long-tape manufacturing.

In figure 7 is shown a correlation between the (Ba + Zr)/Cu content of undoped and 5, 15 mol.% Zr-added REBCO films and the alpha parameter defined from power-law dependence, $I_c \sim H^{-\alpha}$, at 4.2 K and magnetic field range of 14–11 T. The alpha parameter is related to the strength of flux pinning in REBCO superconducting films. It is seen from figure 7 that the alpha parameters of 5% and 15% Zr-added films are substantially higher than that of undoped films. It has been reported that undoped REBCO displays low $\alpha \sim 0.5$ due to the lack of strong c-axis correlated pinning [4, 24].

The observed dependency of α of 5% and 15% Zr-added films on (Ba + Zr)/Cu content is similar to J_c behavior presented in figure 6. The 15% Zr-added films exhibit the highest α parameter but the 5% film show a high α over a wide range of (Ba + Zr)/Cu content. The highest alpha values for 5 and 15 mol.% Zr-added REBCO films are 0.89 and 1.02 at (Ba + Zr)/Cu content of 0.72 and 0.76 respectively. The results shown in figure 7 imply that a large distribution of α parameters reported for REBCO samples with Zr addition could be related to (Ba + Zr)/Cu content.

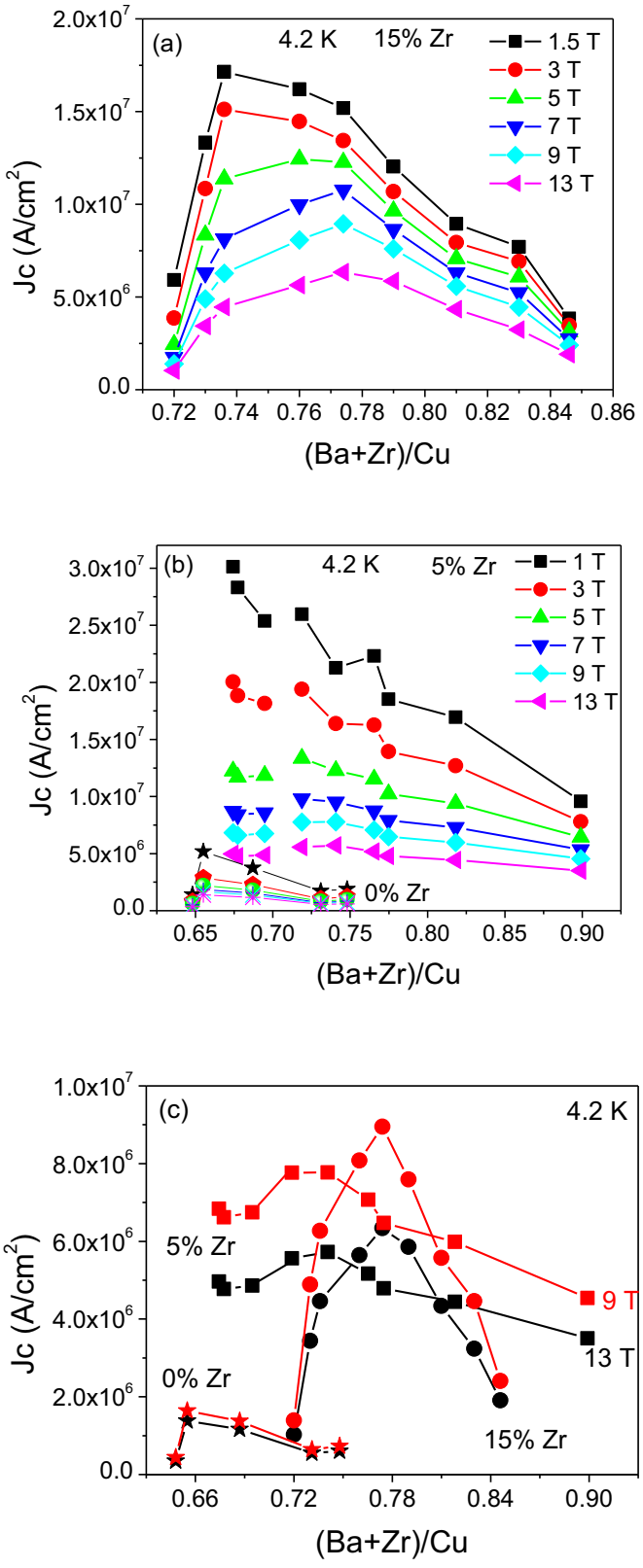

Figure 6. J_c(H) of 15, 5 and 0 mol.% Zr-added REBCO tapes at 4.2 K and B||c as a function of (Ba + Zr)/Cu content. In figure c is shown a comparison of undoped and Zr-added tapes at 9 and 13 T.

In figure 8 is shown the field dependence of pinning force density F_p measured from magnetization critical cur-

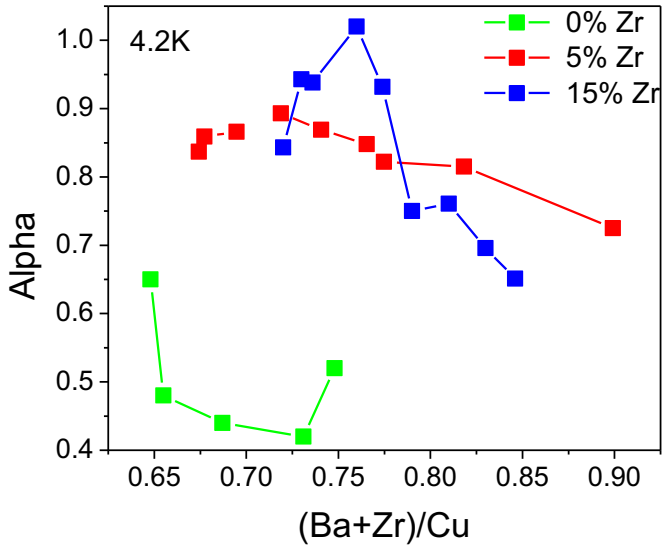

Figure 7. Alpha parameter defined from power-law dependence, $I_c \sim H^{-\alpha}$, at 4.2 K and magnetic field range of 14–11 T as a function of (Ba + Zr)/Cu content of undoped and 5,15 mol. % Zr-added $(Gd,Y)Ba_2Cu_3O_{7-x}$ films.

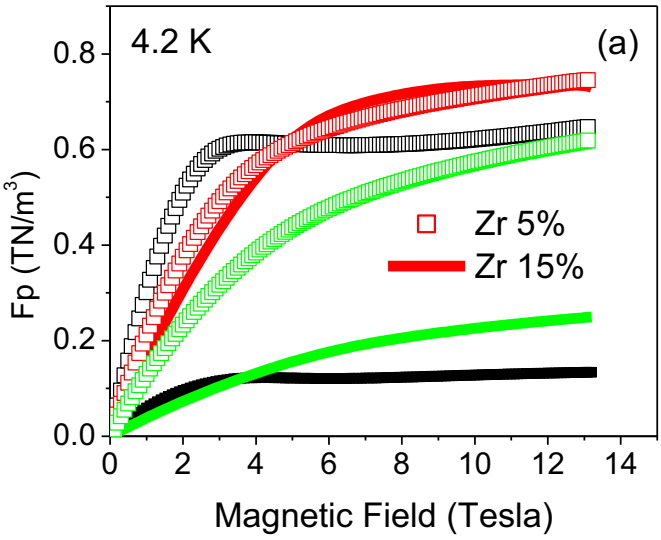

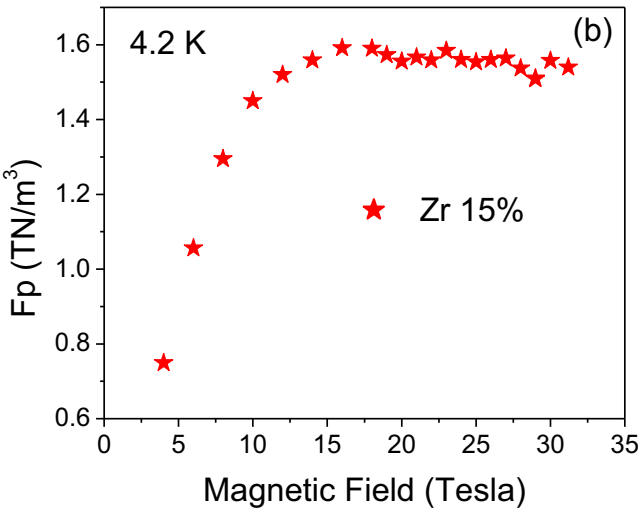

Figure 8. Magnetic pinning force at 4.2 K versus magnetic field applied along the c-axis of 5 (open symbols) and 15 mol.% (solid symbols) Zr-added $(Gd,Y)Ba_2Cu_3O_{7-x}$ films with low (black), intermediate (red) and high (green) (Ba + Zr)/Cu content (a). The transport pinning force density of 15 mol.% Zr-added $(Gd,Y)Ba_2Cu_3O_{7-x}$ with intermediate (Ba + Zr)/Cu content (0.76), as measured at NHMFL (b).

rent density of 5 and 15 mol.% Zr-added samples with different (Ba + Zr)/Cu content. The (Ba + Zr)/Cu content of the 5 mol.% Zr-added samples are 0.674 (low), 0.741 (intermediate) and 0.899 (high). The (Ba + Zr)/Cu content of the 15 mol.% Zr-added samples are 0.72 (low), 0.76 (intermediate) and 0.846 (high).

It can be seen at 13 T the pinning force of 0.7 TN m^{-3} is almost the same value between 5 and 15% Zr films with intermediate (Ba + Zr)/Cu content of 0.74 and 0.776 respectively. The pinning force density values of 5 and 15 mol.% Zr-added samples with low (Ba + Zr)/Cu are 0.57 and 0.14 TN m^{-3} respectively. The pinning force density values of 5 and 15 mol.% Zr-added samples with high (Ba + Zr)/Cu are 0.6 and 0.25 TN m^{-3} respectively. Transport current measurements done at NHMFL on the same 15 mol.% Zr-added sample with intermediate (Ba + Zr)/Cu shows a transport pinning force density of 1.5 TN m^{-3} ($J_c = 11.7$ MA cm^{-2} at 13 T) which is larger than magnetic Fp by factor of 2.1. Previously, record high transport critical current density at 4.2 K and 30 K was reported by our group for optimized 15 and 20 mol.% Zr-added (Gd,Y)BCO films [17, 19, 20]. Another interesting observation is an almost constant transport $F_p = 1.5$ TN m^{-3} over a field range of 16–32 T. The alpha parameter defined from power-law dependence in magnetic and transport measurements in the field range 13–11 T and 32–18 T respectively is almost identical at 1.02 and 1.04.

The normalized pinning force density $f_p = F_p/F_{p\text{-max}}$ at 4.2 K of 5 and 15 mol.% Zr-added REBCO samples with low, intermediate and high (Ba + Zr)/Cu content is presented in figure 9. Both sets of samples with 5 and 15 mol.% Zr show a similar behavior.

The field dependence of F_p of tapes with the lowest (Ba + Zr)/Cu content of 0.674 and 0.72 in 5 and 15 mol.% Zr-added samples respectively shows a quick rise of normalized pinning force density from 0 up to B^*. For samples with the lowest (Ba + Zr)/Cu content the B^* is defined as a field at which the slope of $f_p(H)$ curve changes from high to moderate. For the films with intermediate and high (Ba + Zr)/Cu content, the slope $f_p(H)$ is gradual and the derivative of $f_p(H)$ as shown in figure 9(b) inset is used to precisely define the change in slope. Above B^*, which is 3.9 and 4.2 T for 5 and 15 mol.% Zr-added samples respectively, the normal pinning force density reduces to B_{min} and increases again at a slow rate. The films with intermediate and the highest (Ba + Zr)/Cu content show a shift of B^* to higher fields in the following order: 5 and 5.8 T for 5% Zr samples and 7.8 and 9 T for 15% Zr samples.

The shape of $f_p(H)$ curve at 4.2 K may be affected by orientation, morphology and continuity of BZO nanorods on the. Our earlier published work and current TEM study of Zr-added

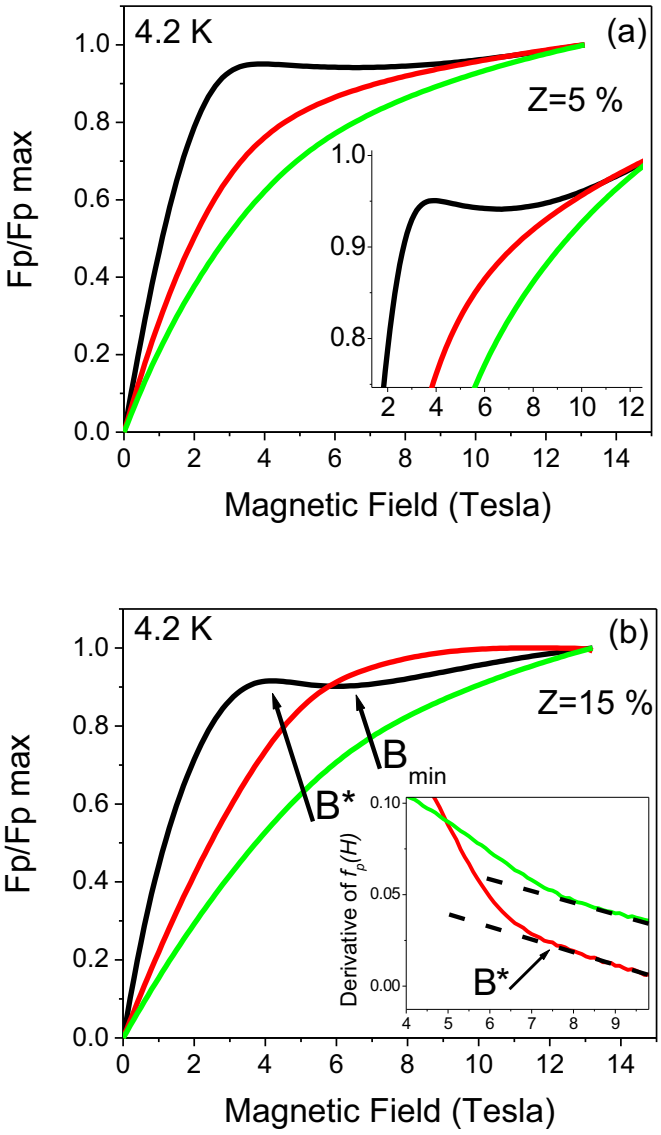

Figure 9. Field dependence of normalized pinning $f_p = F_p/F_{p\,max}$ at 4.2 K for 5(a) and 15(b) mol.% Zr-added REBCO samples with low (black), intermediate (red) and high (green) (Ba + Zr)/Cu content. The inset in figure (a) shows a magnified scale $f_p(H)$ of $(Gd,Y)Ba_2Cu_3O_{7-x}$ with 5 mol.% addition. The inset in figure (b) shows a derivative of $f_p(H)$ where the dashed lines help determine B^*, the field at which the slope changes.

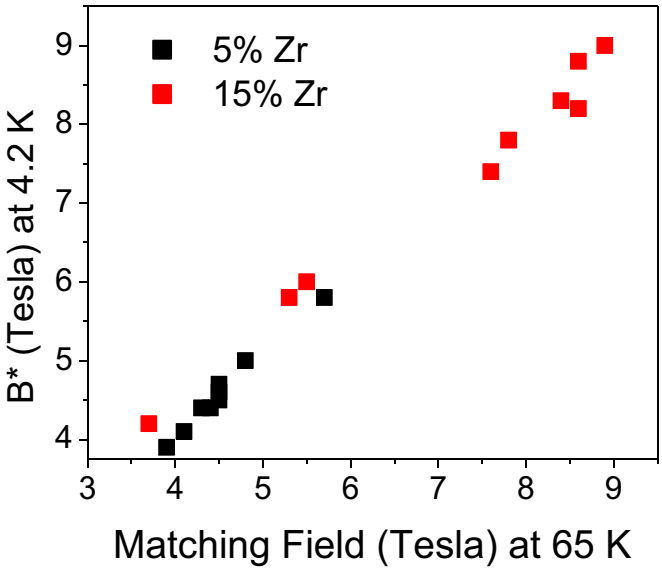

Figure 10. Correlation between characteristic field parameter B^* defined from $F_p(H)$ at 4.2 K and matching field obtained from $F_p(H)$ at 65 K for all 5 and 15 mol.% added REBCO tapes.

samples made by A-MOCVD or conventional MOCVD did not reveal an inclination of BZO nanorods´ growth direction from the *c*-axis orientation of REBCO. Rather, the shape of the $F_p(H)$ curve is likely associated to the segmentation of BZO nanorods by RE_2O_3 in-plane precipitates. As discussed above, an excess of RE content is available for the formation of REO precipitates in Zr-added samples with lowest (Ba + Zr)/Cu content. The appearance of B_{min}, shown in figure 9 has been observed for 5 and 15 mol.% Zr-added samples with lowest (Ba + Zr)/Cu content. A similar unusual shape of $f_p(H)$ curve has been reported by Tsuchia *et al* but at 77 K, for $BaHfO_3$ (BHO)-doped $SmBa_2Cu_3O_{7-\delta}$ [45, 46]. It was explained by delocalization of the vortex, where the mean amplitude of the thermal fluctuation is longer than the distance between the nanorods [47]. We have however not observed the double peak in the $F_p(H)$ curve at 65–77 K in Zr-added films with low (Ba + Zr)/Cu content, at least up 13 T.

Figure 10 shows a linear correlation between B^* defined from $F_p(H)$ at 4.2 K and matching field obtained from $F_p(H)$ at 65 K for all 5 and 15 mol.% Zr added REBCO tapes. It should be noted that the correlation is not only linear, but that the scale factor is unity, i.e. the B^* at 4.2 K and matching field at 65 K are exactly the same. Previously, we had reported that matching fields calculated from the spacing between BZO nanorods is almost the same as the matching fields obtained from normalized $F_p(H)$ curves at 65 K [38]. We can conclude that the pinning mechanisms at 4.2 K and low magnetic fields are mostly governed by BZO nanorods, at least up to B^*. Hence, the characteristic B^* field obtained from $F_p(H)$ at 4.2 K apparently differentiates the cross point between strong correlated pining governed by BZO nanorods and weak uncorrelated pinning.

To further understand the governing pinning mechanisms responsible for the different $F_p(H)$ behavior of 5 and 15 mol.% Zr-added REBCO samples at 4.2 K with low and high (Ba + Zr)/Cu content, we use Dew-Hughes-type functions for the field dependence of the pinning force density [48]. When there are several types of pinning centers in a superconductor, the normalized pinning force can be described by:

$$f = Ab^p(1-b)^q,$$

where A is constant, $b = B/B_{irr}$ is the reduced magnetic field and the variables p and q are parameters that are associated with the flux pinning mechanism in the original model. Because the actual irreversibility field B_{irr} is difficult to determine especially at lower temperatures, the Kramer plot has been used to define B_{irr} through extrapolation of

the $J_c^{0.5}(B)^{0.25}$ curve to zero [49]. The high field region is mostly described by q parameter. In this region, the repulsive vortex-vortex interaction begins to be the main determining factor. According to Dew-Hughes, the normalized vortex pinning forces $f = F_P/F_p^{\max}$ at different temperatures will collapse to one curve if there is a dominant pinning mechanism [48]. We found that one term equation representing a single pinning species cannot adequately fit the data for Zr-added (Gd,Y)$Ba_2Cu_3O_{7-x}$ samples because of the different type of defects such as nanorods and nanoparticles that contribute to pinning in these samples. We found that $= Ab^{p1}(1-b)^{q1} + Bb^{p2}(1-b)^{q2}$ a two-component model, combined additively, gives a reasonable fit for 5 and 15 mol.% Zr-added (Gd,Y)$Ba_2Cu_3O_{7-x}$ samples with the lowest, intermediate and largest (Ba + Zr)/Cu content. For example, figure 11 shows the field dependence of normalized pinning force $f = F_P/F_p^{\max}$ as a function of normalized magnetic field $b = B/B_{irr}$ for 15 mol.% Zr-added film with the lowest (Ba + Zr)/Cu = 0.72 content at 4.2 and 77 K. The values of p1 and q1 for the pinning centers of interest are given by Dew-Hughes, and will be discussed below, while parameters p2 and q2 are fitting parameters only. In the Dew-Hughes analysis the parameter p = 1 is related to core pinning (pinning center dimension less than the penetration depth) by point-like normal-state particles. The parameter p1 obtained with the two component model for all 5 and 15 mol.% REBCO samples over a temperature range of 77–4.2 K is in the range of 0.9–1.1. This pinning mechanism is consistent with the 4–6 nm diameter $BaZrO_3$ particles observed in the TEM micrograph in figure 3. However, the obtained parameter q1 which represents the high field region is different for samples with low and high (Ba + Zr)/Cu content at temperatures below 30 K (q1 > 10 for samples with low (Ba + Zr)/Cu content and q1 ∼ 2 for samples with high (Ba + Zr)/Cu content), while it is nearly the same q1 ∼ 2 at high temperatures (30–77 K) for all samples.

It is recognized that the peak positions of F_p/F_p max curves point to the pinning mechanism and could be determined as $b_{\max} = p/(p+q)$ [48]. For REBCO, it has been found that $b_{\max}$ is in the range of 0.33 to 0.5, which is in accordance with pinning provided by normal-conducting or insulating regions [50]. The reported variation of $b_{\max}$ is attributed to different RE_2O_3 particles [50]. In figure 12 is shown the temperature dependence of $b_{\max} = p1/(p1+q1)$ for undoped sample with the lowest Ba/Cu (0.648), 5 and 15 mol.% Zr-added REBCO films with the lowest (Ba + Zr)/Cu (0.67 and 0.72 respectively), intermediate (Ba + Zr)/Cu (0.74 and 0.774) and the highest (Ba + Zr)/Cu (0.89 and 0.84). It can be seen that for undoped sample, $b_{\max}$ is temperature independent and equal to 0.12. For REBCO with 5 and 15 mol.% Zr addition and the highest (Ba + Zr)/Cu, $b_{\max}$ is around 0.3 over the entire temperature range of 4.2–77 K. This may be due to a monotonous microstructure of continuous $BaZrO_3$ nanorods without interference by RE_2O_3 precipitates in films with high (Ba + Zr)/Cu as seen in figure 3(c).

The 5 and 15 mol.% Zr-added samples with the lowest and intermediate (Ba + Zr)/Cu content show $b_{\max} \sim 0.31$ and $b_{\max} \sim 0.33$ at 65 and 77 K. At lower temperatures of 30 and 4.2 K, the 5 and 15 mol.% Zr-added films with the lowest

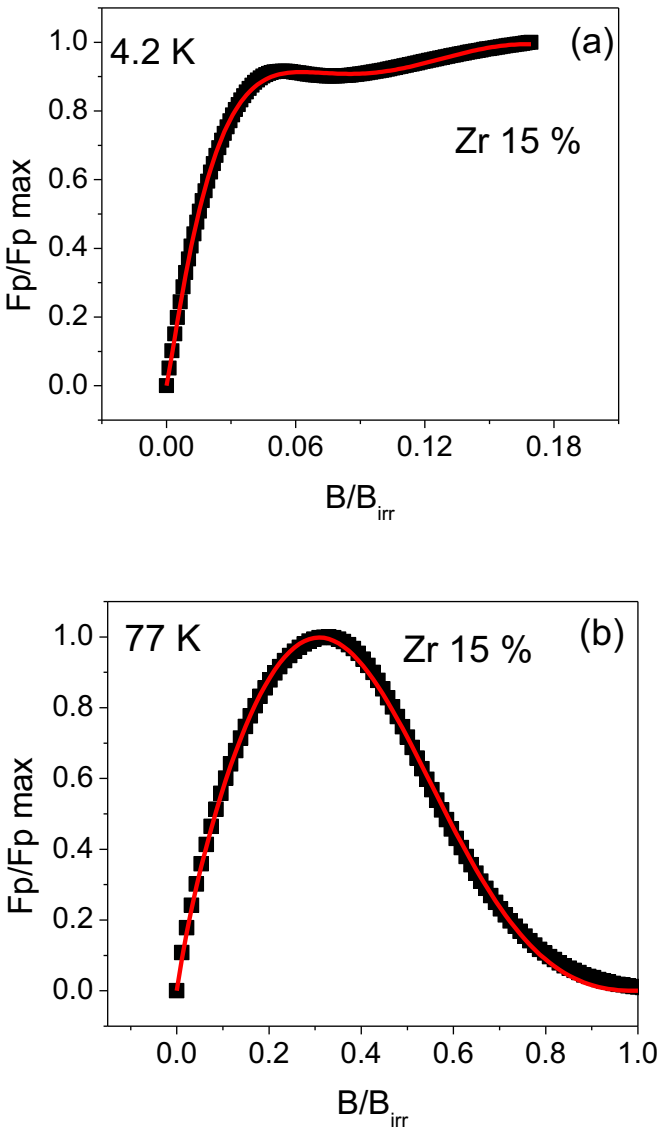

Figure 11. The scaled pinning force density $f = F_P/F_p^{\max}$ as a function of the reduced field $b = B/B_{irr}$ and fitting curve of 15 mol.% Zr-added film with the lowest (Ba + Zr)/Cu of 0.72 content, at 4.2 K (a) and 77 K (b).

(Ba + Zr)/Cu content show $b_{\max} \sim 0.08$ and 0.05 respectively, while the films with intermediate (Ba + Zr)/Cu content show $b_{\max} \sim 0.23$ and 0.18. We found that at 4.2 K the b_{max} for Zr added tapes with the lowest (Ba + Zr)/Cu content is different than b_{max} for the samples with intermediate and high (Ba + Zr)/Cu content, while at temperature above 30 K where correlated pinning dominates, the b_{max} is similar for all samples. Apparently, the b_{max} characterizing the weak pinning mechanism at low temperature is affected by density, diameter and morphology of BZO nanorods and other inclusions such as RE_2O_3 which is controlled by the (Ba + Zr)/Cu content.

Based on microstructure evidence of high density of in-plane RE_2O_3 precipitates interfering with the BZO nanorods (figure 3(a)) and observed anomaly (B_{min}) in the field dependence of pinning force density at 4.2 K (figure 9) in REBCO with low (Ba + Zr)/Cu, we attribute the lower $b_{\max}$

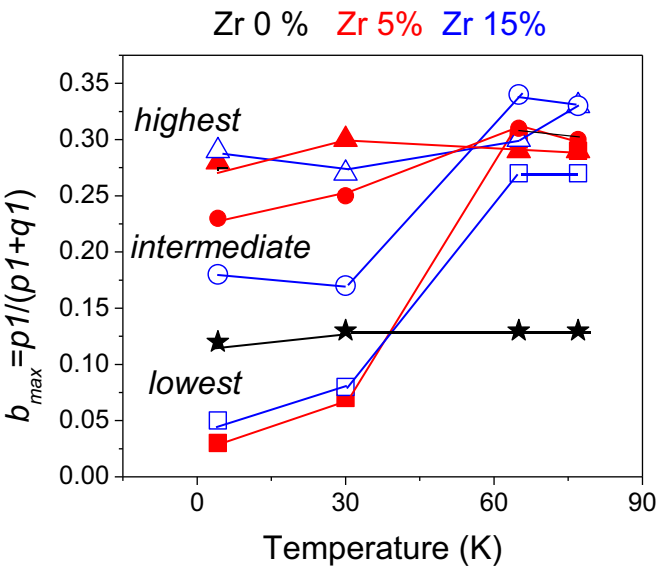

Figure 12. The temperature dependence of $b_{max} = p1/(p1 + q1)$ for undoped (star symbol), 5 and 15 mol.% Zr−added $(Gd,Y)Ba_2Cu_3O_{7-x}$ films with the lowest (square symbol), intermediate (circular symbol) and the highest (triangle symbol) (Ba + Zr)/Cu content.

at lower temperatures in these samples to the weak pinning mechanisms that are different from those in samples with high (Ba + Zr)/Cu content. The strain-field distribution in REBCO that is considered to be responsible for weak pinning could be influenced by the segmentation of the nanorods by REO precipitates in films with low (Ba + Zr)/Cu content.

4. Conclusion

We have studied the critical current density and pinning mechanisms of 0, 5 and 15 mol.% Zr-added 4+ μm REBCO tapes fabricated by A-MOCVD. We found that in addition to the amount of Zr addition, the Ba content in the film also strongly affects the critical current of the tapes. Microstructure analyses reveals a correlation between (Ba + Zr)/Cu content with density, continuity and shape of $BaZrO_3$ nanorods, which act as effective correlated pinning centers along *c*-axis and are a source of weak point defects that enhance the J_c over a wide range of magnetic fields at 4.2 K. We found that at 4.2 K and high magnetic fields of 7–13 T, the critical current density and alpha parameter show a bell-shape behavior as a function of (Ba + Zr)/Cu content. From $F_p(H)$ behavior at 4.2 K, we have defined a characteristic B^* field parameter which apparently shows a transition between strong correlated pinning governed by BZO nanorods and weak uncorrelated pinning by points defects. Additionally, fitting of the pinning force density $F_p(H)$ by a two-component Dew–Hughes model shows the scaling characteristics of strong and weak pinning centers.

Acknowledgments

This work was supported by the US Department of Energy (DOE) Office of High Energy Physics award DE-SC0016220.

A portion of this work was performed at the National High Magnetic Field Laboratory, which is supported by National Science Foundation Cooperative Agreement No. DMR-1644779 and the state of Florida.

ORCID iDs

Eduard Galstyan https://orcid.org/0000-0003-1486-6449
Goran Majkic https://orcid.org/0000-0003-0168-0856
Mehdi Kochat https://orcid.org/0000-0002-2928-0718
Jan Jaroszynski https://orcid.org/0000-0003-3814-8468
Venkat Selvamanickam https://orcid.org/0000-0001-6618-9406

References

[1] Bruzzone P, Fietz W H, Minervini J V, Novikov M, Yanagi N, Zhai Y and Zheng J 2018 High temperature superconductors for fusion magnets *Nucl. Fusion* **58** 103001
[2] Atomura N, Takahashi T, Chiba Y, Tsuda M, Hamajima T, Shikimachi K, Hirano N and Nagaya S 2011 Homogeneous current distribution experiment in a multi-laminated HTS tape conductor for a double-pancake coil of SMES *Physcia* C **471** 1396–8
[3] Larbalestier D, Gurevich A, Feldmann D M and Polyanskii A 2001 High-Tc superconducting materials for electric power applications *Nature* **414** 368–77
[4] Eisterer M, Moon S H and Freyhardt H C 2016 Current developments in HTS coated conductors for applications *Supercond. Sci. Technol.* **29** 060301
[5] Braccini V *et al* 2011 Properties of recent IBAD-MOCVD coated conductors relevant to their high field, low temperature magnet use *Supercond. Sci. Technol.* **24** 035001
[6] Kar S, Luo W and Selvamanickam V 2017 Ultra-small diameter round REBCO wire with Robust Mechanical properties *IEEE Trans. Appl. Supercond* **27** 6603204
[7] Iwasa Y and Hahn S 2013 First-cut design of an all superconducting 100-T direct current magnet *Appl. Phys. Lett.* **103** 253507
[8] Yoon S, Kim J, Lee H and Hahn S 2016 26 T 35 mm all-$GdBa_2Cu_3O_{7-}x$ multi-width no-insulation superconducting magnet *Supercond. Sci. Technol.* **29** 04LT04
[9] Maeda H and Yanagisawa Y 2014 Recent developments in high-temperature superconducting magnet technology *IEEE Trans. Appl. Supercond.* **24** 4602412
[10] Xu A, Selvamanickam V, Jaroszynski J, Kametani F and Larbalestier D C 2014 Strongly enhanced vortex pinning from 4 to 77 K in magnetic fields up to 31 T in 15 mol% Zr added (Gd, Y)-Ba–Cu–O superconducting tapes *APL Mater.* **2** 046111
[11] Miura S, Yoshida Y, Ichino Y, Xu Q, Matsumoto K, Ichinose A and Awaji S 2016 Improvement in Jc performance below liquid nitrogen temperature for $SmBa_2Cu_3O_y$ superconducting films with $BaHfO_3$ nano-rods controlled by low-temperature growth *APL Mater.* **4** 016102
[12] Ino Ue M *et al* 2016 Enhancement of In-field current transport properties in GdBCO coated conductors by $BaHfO_3$ doping *IEEE Trans. Appl. Supercond.* **23** 8002304
[13] Tobita H, Notoh K, Higashikawa K, Inoue M, Kiss T, Kato T, Hirayama T, Yoshizumi M, Izumi T and Shiohara Y 2012 Fabrication of $BaHfO_3$ doped $GdBa_2Cu_3O_{7-\delta}$ coated conductors with the high Ic of 85 A/cm-w under 3 T at

liquid nitrogen temperature (77 K) *Supercond. Sci. Technol.* **25** 062002
[14] MacManus-Driscoll J L, Foltyn S R, Jia Q X, Wang H, Serquis A, Civale L, Maiorov B, Hawley M E, Maley M P and Peterson D E 2004 Strongly enhanced current densities in superconducting coated conductors of $YBa_2Cu_3O_{7-x}$ + $BaZrO_3$ *Nat. Mater* **3** 439–43
[15] Matsumoto K and Mele P 2010 Artificial pinning center technology to enhance vortex pinning in YBCO coated conductors *Supercond. Sci. Technol.* **23** 014001–12
[16] Gharahcheshmeh M H, Majkic G, Galstyan E, Xu A, Zhang Y, Li X-F and Selvamanickam V 2018 Control of in-field performance of 25 mol.% Zr-added REBCO superconductor tapes *Physica* C **553** 26
[17] Majkic G, Pratap R, Xu A, Galstyan E and Selvamanickam V 2018 Over 15 MA/cm^2 of critical current density in 4.8 μm thick, Zr-doped (Gd,Y)Ba2Cu3Ox superconductor at 30 K, 3T *Sci. Rep.* **8** 6982
[18] Miura S, Yoshida Y, Ichino Y, Matsumoto K, Ichinose A and Awaji S 2015 Characteristics of high-performance $BaHfO_3$-doped $SmBa_2Cu_3O_y$ superconducting films fabricated with a seed layer and low-temperature growth *Supercond. Sci. Technol.* **28** 065013
[19] Xu A *et al* 2017 *Je*(4.2 K, 31.2 T) beyond 1 kA/mm^2 of a ∼3.2 μm thick, 20 mol.% Zr added MOCVD REBCO coated conductor *Sci. Rep.* **7** 6853
[20] Majkic G, Rudra P, Xu A, Galstyan E, Higley H C, Prestemon S O, Wang X, Abraimov D, Jaroszynski J and Selvamanickam V 2018 Engineering current density over 5 kAmm^{-2} at 4.2 K, 14 T in thick film REBCO tapes *Supercond. Sci. Technol.* **31** 10LT01
[21] Majkic G, Galstyan E and Selvamanickam V 2015 High performance 2G-HTS wire using a novel MOCVD system *IEEE Trans. Appl. Supercond.* **25** 1–4
[22] Majkic G, Rudra P, Galstyan E, Xu A, Zhang Y and Selvamanickam V 2017 Engineering of nanorods for superior in field performance of 2G-HTS conductor utilizing advanced MOCVD reactor *IEEE Trans. Appl. Supercond.* **27** 1–5
[23] Xu A, Braccini V, Jaroszynski J, Xin Y and Larbalestier D C 2012 Role of weak uncorrelated pinning introduced by $BaZrO_3$ nanorods at low-temperature in (Y,Gd)$Ba_2Cu_3O_x$ thin films *Phys. Rev.* B **86** 115416
[24] Polat O, Sinclair J W, Zuev Y L, Thompson J R, Christen D K, Cook S W, Kumar D, Chen Y and Selvamanickam V 2011 Thickness dependence of magnetic relaxation and E-J characteristics in superconducting (Gd-Y)-Ba-Cu-O films with strong vortex pinning *Phys. Rev.* B **84** 024519
[25] Gharahcheshmeh M H, Galstyan E, Xu A, Kukunuru J, Katta R, Zhang Y, Majkic G, Li X-F and Selvamanickam V 2017 Superconducting transition width (ΔT_c) charcteristics of 25 mol.% Zr-added (Gd,Y)$Ba_2Cu_3O_{7-\delta}$ superconductor tapes with high in-field critical current density at 30K *Supercond. Sci. Technol.* **30** 015016
[26] Bean C P 1965 Magnetization of high-field superconductors *Rev. Mod. Phys.* **36** 31
[27] Campbell A M and Evetts J E 1972 Flux vortices and transport currents in type II superconductors *Adv. Phys.* **21** 199
[28] Thompson J R, Polat O, Christen D K, Kumar D, Martin P M and Sinclair J W 2008 Wide-range characterization of current condition in high-Tc coated conductors *Appl. Phys. Lett.* **93** 042506
[29] Majkic G, Rudra P, Galstyan E and Selvamanickam V 2019 Correlation of in-field performance of thick REBCO films between 0-14 T and 4. 2-77K *IEEE Trans. Appl. Supercond.* **29** 6602005
[30] Selvamanickam V, Heydari Gharahcheshmeh M, Xu A, Zhang Y and Galstyan E 2015 Requirements to achieve high in-field critical current density at 30 K in heavily-doped (Gd,Y)$Ba_2Cu_3O_{-x}$ superconductor tapes *Supercond. Sci. Technol.* **28** 104003
[31] Galstyan E, Heydari Gharahcheshmeh M, Delgado L, Xu A, Majkic G and Selvamanickam V 2015 Microstructure characteristics of high lift factor MOCVD REBCO coated conductors with high Zr content *IEEE Trans, Appl. Supercond.* **25** 6604305
[32] Selvamanickam V *et al* 2013 Enhanced critical currents in (Gd,Y)$Ba_2Cu_3O_x$ superconducting tapes with high levels of Zr addition *Supercond. Sci. Technol.* **26** 035006
[33] MacManus-Driscoll J L, Alonso J A, Wang P C, Geballe T H and Bravman J C 1994 Studies of structural disorder in $ReBa_2Cu_3O_{7-x}$ thin films (Re-rare earth) as a function of rare-earth ionic radius and film deposition condition *Physica* C **232** 288
[34] Selvamanickam V, Chen Y, Zhang Y, Guevara A, Shi T, Yao Y, Majkic G, Lei C, Galstyan E and Miller D J 2012 Effect of rare-earth composition on microstructure and pinning properties of Zr-doped (Gd,Y)$Ba_2Cu_3O_{7-x}$ superconducting tapes *Supercond. Sci. Technol.* **25** 045012
[35] Wu J, Shi J, Baca J, Emerge R, Haugan T, Maiorov B and Holesinger T 2014 The effect of lattice strain on the diameter of BaZrO3 nanorods in epitaxial $YBa_2Cu_3O_{7-\delta}$ films *Supercond. Sci. Technol.* **27** 044010
[36] Kim S I, Kametani F, Chen Z, Gurevich A, Larbalestier D C, Haugan T and Barnes P 2007 On the through-thickness critical current density of an $YBa_2Cu_3O_{7-x}$ film containing a high density of insulating, vortex-pinning nanoprecipitates *Appl. Phys. Lett.* **90** 252502
[37] Mele P *et al* 2015 High pinning performance of $YBa_2Cu_3O_{7-x}$ films added with Y_2O_3 nanoparticulate defects *Supercond. Sci. Technol.* **28** 024002
[38] Galstyan E, Pratap P, Majkic G, Kochat M, Mohan V and Selvamanickam V 2018 Correlation between microstructure and in-field performance of Zr-added REBCO coated conductors made by advanced MOCVD *IEEE Trans, Appl. Supercond.* **29** 8001206
[39] Augieri A *et al* 2010 Pinning analyses epitaxial on YBa2Cu3O7− δ films with BaZrO3 inclusions *J. Phys. D: Appl. Phys.* **108** 063906
[40] Gutiérrez J, Puig T and Obradors X 2007 Anisotropy and strength of vortex pinning centers in $YBa_2Cu_3O_{7-x}$ coated conductors *Appl. Phys. Lett.* **90** 162514
[41] Senatore C, Barth C, Bonura M, Kulich M and Mondonico G 2015 Field and temperature scaling of the critical current density in commercial REBCO coated conductors *Supercond. Sci. Technol.* **29** 014002
[42] Horide T, Kametani F, Yoshioka S, Kitamura T and Matsumoto K 2017 Structural evolution induced by interfacial lattice mismatch in self-organized $YBa_2Cu_3O_{7-\delta}$ nanocomposite film *ACS Nano* **11** 1780–8
[43] Werner M, Sauerzopf F M, Weber H W and Wisniewski A 2000 Fishtail effect in the magnetization of superconducting $RBa_2Cu_3O_{7-\delta}$ (R=Y, Nd, Yb) and $Y_2Ba_4Cu_8O_{16}$ single crystals *Phys. Rev.* B **61** 14795
[44] Daeumling M, Seuntjens J M and Larbalestier D C 1990 Oxygen-defect flux pinning, anomalous magnetization and intra-grain granularity in $YBa_2Cu_3O_{7-\delta}$ *Nature* **346** 332
[45] Tsuchiya Y, Awaji S, Watanabe K, Miura S, Ichino Y, Yoshida Y and Matsumoto K 2016 Delocalization of vortex in SmBa2Cu3O7−δ superconducting films with BaHfO3 nanorods *J. Phys. D: Appl. Phys.* **120** 103902
[46] Tsuchiya Y, Miura S, Awaji S K, Ichino Y, Ichino Y, Matsumoto K, Izumi T, Watanabe K and Yoshida Y 2017 Flux pinning landscape up to 25 T in SmBa2Cu3O7−δ films with BaHfO3 nanorods fabricated by low-temperature grow technique Supercond *Sci. Technol.* **30** 104004

[47] Blatter G, Geshkenbein V B, Larkin A I and Vinokur V M 1994 Vortices in high-temperature superconductors *Rev. Mod. Phys.* **66** 1125–388
[48] Dew-Hughes D 1974 Flux pinning mechanisms in type II superconductors *Phil. Mag.* **30** 293
[49] Kramer E J 1973 Scaling laws for flux pinning in hard superconductors *J. Appl. Phys.* **44** 1360–70
[50] Koblishchka M R and Murakami M 2000 Pinning mechanisms in bulk high Tc- superconductors *Supercond. Sci. Technol.* **13** 738